Processing and Application of Ceramics 15 [1] (2021) 19–31
https://doi.org/10.2298/PAC2101019O


# Microstructure and electrical conductivity of 3Y-TZP/$Al_2O_3$ composites

Katarzyna Obal[1], Jan Wyrwa[1], Andrzej Kruk[2], Małgorzata Dziubaniuk[1], Zbigniew Pędzich[1], Mieczysław Rękas[1], Tomasz Brylewski[1,*]

[1]*AGH University of Science and Technology, Faculty of Materials Science and Ceramics, al. Mickiewicza 30, 30-059 Krakow, Poland*
[2]*Pedagogical University of Krakow, Institute of Technology, ul. Podchorążych 2, 30-084 Kraków, Poland*

Received 24 June 2020; Received in revised form 17 November 2020; Accepted 28 December 2020

## Abstract

*Various amounts of $Al_2O_3$ (0.25, 0.5 and 1.0 mol%) were added to tetragonal polycrystalline material (3Y-TZP), prepared using the hydrothermal crystallization method. The effects of the added amount as well as the sintering temperature on the microstructure and electrical properties of the 3Y-TZP/$Al_2O_3$ composites were investigated. The alumina addition was found to affect the microstructure of the 3Y-TZP samples obtained after sintering at 1400 or 1500 °C only to a slight extent. The lowest values of the blocking factor, which represents the contribution of grain boundary resistivity to the total resistivity of a polycrystal, were observed for the 3Y-TZP with $Al_2O_3$ additions of 0.25 or 0.5 mol% at measurement temperatures of 550 and 600 °C. The study proves that the 3Y-TZP/$Al_2O_3$ should be taken into consideration as solid electrolyte in the intermediate-temperature solid oxide fuel cells.*

***Keywords:*** *zirconia, grain size, microstructure, electrical conductivity, impedance spectroscopy*

## I. Introduction

Many types of fuel cells that differ in terms of their construction and operating conditions have been designed in recent years [1]. Among them, planar solid oxide fuel cells (SOFCs) seem to have the best prospects for future commercialization, since they do not require the use of noble metals, especially platinum, as electrode materials and catalysts [1].

The solid electrolyte is one of the key components of a solid oxide fuel cell. The role of the electrolyte is to transport oxygen ions generated at the cathode towards the anode while the electrons flowing through the external circuit generate electricity. The electrolyte also separates the fuel from the oxidant. The electrolyte material must therefore exhibit chemical stability in both oxidizing and reducing atmospheres, non-permeable to gases, and to be characterized by the highest possible ionic conductivity and the lowest possible electronic conductivity over a wide range of oxygen partial pressures. Last but not least, it has to be thermochemically compatible with the remaining components of a fuel cell stack, i.e. the cathode, the anode, and the interconnect, both at room temperature and over the temperature range of the cell's operation.

Fully stabilized zirconia (FSZ) is commonly applied as a solid oxide electrolyte owing to its suitably high ionic conductivity and considerable chemical stability when in contact with cathode and anode materials in an oxidizing-reducing atmosphere. The commercial application of SOFCs with an FSZ electrolyte is nevertheless limited due to its low mechanical strength, poor resistance to thermal shocks, and overly high temperatures at which fuel cells operate, i.e. 700–800 °C for anode-supported SOFCs with a thin 8-YSZ (FSY) electrolyte, and above 850 °C for 8-YSZ-electrolyte-supported cells [1].

The development of intermediate-temperature solid oxide fuel cells (IT-SOFCs), which are capable of high-output operation at temperatures ranging from 600 to 800 °C is the strategic objective of many institutions which specialize in hydrogen energy. Prospective solutions include the application of tetragonal zirconia polycrystals partially stabilized with 3 mol% of yttria (3Y-TZP) as a substitute for FSZ. The reasons for the appli-

* Corresponding author: tel: +48 12 6175229,
e-mail: *brylew@agh.edu.pl*

cation of 3Y-TZP as an IT-SOFC electrolyte include not only its significantly higher mechanical strength and resistance to thermal shocks [2], but also its lower activation energy of electrical conduction and its subsequently higher electrical conductivity at temperatures below 700 °C [3]. The research conducted thus far shows that in such conditions the electrical conductivity of grains is higher in 3Y-TZP than in FSZ [3]. Regardless of this, the total electrical conductivity of the 3Y-TZP polycrystalline material is lower due to the high electrical resistance at grain boundaries [4–6]. The literature on the subject refers to this phenomenon using the term "blocking effect" [4–6]. As a result of impurities that segregate in this area, most notably silica, a thin insulating layer forms; this layer inhibits the migration of oxygen ions across grain boundaries [7]. It was found that when $Al_2O_3$ is added in an amount exceeding its solubility limit in the 3Y-TZP material, it acts as a "scavenger" of silicon compounds [8–11]. One such material is the 3Y-TZP composite containing 0.5 mol% of $Al_2O_3$, which was prepared using a 3-YSZ powder obtained via co-precipitation and sintering at 1500 °C; the high electrical conductivity of grain boundaries allows this material to exhibit a low blocking factor [12].

The removal of silica from grain boundaries occurs when it binds with alumina and forms mullite, as expressed by the following equation proposed by Butler and Drennan [8]:

$$3\,Al_2O_3 + 2\,SiO_2 \rightleftharpoons Al_6Si_2O_{13} \qquad (1)$$

A consequence of this reaction is an increase in the electrical conductivity across grain boundaries [10]. On the other hand, when alumina is added in an amount lower than the solubility limit, it has a slightly negative effect on the electrical conductivity of grains, and a considerable, likewise negative effect on the grain boundary electrical conductivity in the 3Y-TZP material [7,13]. This is explained by the drop in the concentration of oxygen vacancies in the space charge layer, associated with an increased Schottky barrier, which effectively increases the activation energy of conduction in the space charge zone [7].

The results of the research published on the influence of $Al_2O_3$ addition on the electrical conductivity of 3Y-TZP are often contradictory. Some authors report increased electrical conductivity [14], while others report the opposite [15]. According to Guo *et al.* [16], the aluminium ions originating from $Al_2O_3$ form defect complexes with oxygen vacancies in 3Y-TZP structure, thus modifying the Schottky barriers at grain boundaries. According to current knowledge, the effect of alumina addition on electrical conductivity seems to depend not only on its concentration, but also the way in which the tetragonal form of zirconia in the 3Y-TZP/$Al_2O_3$ is obtained and, subsequently, in which its microstructure is modified.

Another potential method for improving the conducting properties of 3Y-TZP is to manufacture this material from nanopowder instead of the commonly applied material with micron-sized grains. Nanomaterials can transport mass in different ways owing to their increased grain boundary surface and a defect thermodynamics that is different than what is observed for the micron-sized counterparts. Some papers [17–19] argue that the concentration of oxygen vacancies on the surface of nanocrystalline particles is higher than in the grain interior. This leads to the conclusion that the electrical conductivity of grain boundaries may be twice as high for materials with nano-sized grains as for those with micron-sized grains. In summary, the influence of alumina on the electrical properties of tetragonal zirconia has not been fully understood.

The aim of the present work was to determine how the addition of $Al_2O_3$, which is an insulator itself, affects the ionic conductivity of the 3Y-TZP material. Since the electrical properties of the tetragonal form of zirconia are a function of its microstructure, two variables were considered especially significant from the perspective of obtaining a 3Y-TZP electrolyte with the most desirable physicochemical parameters: i) the amount of alumina added to the 3-YSZ powder prepared via hydrothermal crystallization, and ii) the temperature at which the samples were sintered. Since previous investigations had confirmed the advantageous effect of adding 0.5 mol% of alumina to the 3Y-TZP material obtained using a 3-YSZ powder prepared via co-precipitation on the electrical conductivity of grain boundaries and grains [12], the amounts selected for the present study were 0.25, 0.5 and 1.0 mol%.

## II. Experimental

### *2.1. Preparation of 3Y-TZP/$Al_2O_3$ samples*

$Y_2O_3$-$ZrO_2$ solid solution powder containing 3 mol% of $Y_2O_3$ (3-YSZ) was obtained from analytical-grade zirconium oxychloride ($ZrOCl_2$) and analytical-grade yttria ($Y_2O_3$), while an analytical-grade aqueous solution of ammonia served as the precipitating agent; all reagents used for this reaction were supplied by POCH-Gliwice.

The powder was synthesized in the exact same way in which the preparation of the 8-YSZ powder, described in Ref. [20], had been performed. The obtained co-precipitation product underwent hydrothermal crystallization in an experimental stand consisting of an autoclave and a heater [21]. The autoclave had the shape of a cylinder made from stainless steel, and it was sealed using a stainless steel plug. The gel was inserted into the autoclave in a special teflon container to protect it from impurities and crystallization was carried out at 240 °C for 2 h. This temperature corresponds to an autogenous water vapour pressure of ca. 4 MPa.

The obtained 3-YSZ powder was placed in a Büchner funnel and rinsed with an isopropyl alcohol solution to prevent the formation of agglomerates, and then milled in an attrition mill for 2 h. The grinding process

was carried out in an acetone medium, with zirconia milling balls.

The obtained 3-YSZ powder was impregnated using an alcohol solution of aluminium nitrate with the appropriate concentration established by means of ICP-OES (OPTIMA 7300 DV, Perkin Elmer). During this process, the powder was placed in a glass container filled with an $Al(NO_3)_3$ solution and vigorously mixed at room temperature for 24 h using a magnetic stirrer. These suspensions were subsequently evaporated until dry powders remained. The powders were then calcined at 750 °C for 2 h in order to decompose the aluminium nitrate into $Al_2O_3$. As a result, three types of 3-YSZ mixtures containing 0.25, 0.5 and 1.0 mol% of $Al_2O_3$ were obtained. These mixtures were then heated up to 800 °C in air, at a rate of 10 °C/min, for 1 h. In order to eliminate the impact of microstructural changes related solely to the performed thermal treatment, the initial 3-YSZ powder was heated under the same conditions and treated as the reference sample.

The powder was then uniaxially pressed under a pressure of 100 MPa to form green bodies. In the subsequent stage, the green bodies underwent cold isostatic pressing (CIP) under a pressure of 250 MPa and were sintered freely. The thermal treatment process involved heating the samples in air, at a rate of 5 °C/min, and then 2 h of sintering at either 1400 or 1500 °C. This procedure yielded two series of samples with the following compositions: 3Y-TZP/0.25 mol% of $Al_2O_3$ (referred to as 3Y-TZP/0.25$Al_2O_3$), 3Y-TZP/0.5 mol% of $Al_2O_3$ (referred to as 3Y-TZP/0.5$Al_2O_3$), 3Y-TZP/1.0 mol% of $Al_2O_3$ (referred to as 3Y-TZP/1.0$Al_2O_3$) and 3Y-TZP as the reference samples. The obtained samples had the form of pellets with a diameter of 7.84–7.92 mm and a thickness of 1.61–1.67 mm, and they were stored in a desiccator.

### 2.2. Characterization methods

The phase composition and the lattice parameters of the samples were evaluated using X-ray diffraction performed by means of the PANalytical X'Pert Pro diffractometer, with the use of Cu$K\alpha$ monochromatic radiation. The qualitative phase composition of the prepared materials was established by comparing the obtained diffraction patterns with the data included in the ICSD database. The amount of each phase and its lattice parameter were determined using the Rietveld method and the HighScore Plus application. All samples examined during the XRD analysis were specimens, which had undergone 1 h of thermal treatment at a temperature 100 °C lower than the sintering temperature in order to remove deformations sustained as a result of grinding and polishing.

Crystallite size in the powder was calculated using the Scherrer equation [22]:

$$D_{XRD} = \frac{K \cdot \lambda}{\beta \cos\theta} \tag{2}$$

where $D_{XRD}$ is crystallite diameter, $\lambda$ is wavelength of incident X-rays (Cu$K\alpha_1$; $\lambda = 0.15406$ nm), $\theta$ is diffraction angle, $K$ is constant (0.9) and $\beta$ is corrected full width at half maximum (FWHM) of the diffraction peak. Crystallite size was established based on the broadening of diffraction peak 101 of the tetragonal form of $ZrO_2$.

The particle size distribution of the powder was determined using a Mastersizer laser particle size analyser, while their specific surface area was established using the BET procedure based on the physical sorption of $N_2$ at liquid nitrogen temperature performed by means of Nova 1200e apparatus manufactured by Quantachrome Instruments. The specific surface area values were used to calculate the equivalent mean BET particle size $d_{BET}$ (assuming their uniform spherical shape) from the following dependence:

$$d_{BET} = \frac{6}{\rho_{XRD} \cdot S} \tag{3}$$

where $S$ is specific surface area of the sample and $\rho_{XRD}$ is X-ray density of the sample.

Morphological observations of the powder and the fracture cross-sections of the samples combined with chemical composition analyses of selected micro-areas were performed by a FEI Nova NanoSEM 200 scanning electron microscope coupled with an energy-dispersive X-ray spectroscopic (EDAX) analyser. The polished cross-sections were thermally etched at 800 °C for 1 h. The obtained SEM micrographs underwent computer binarization and analytical processing with the use of the ImageJ 3.14 application in order to determine the grain diameter and circularity. The grain diameter was defined as the diameter of a disc with a surface area equal to the measured surface area of the grain.

The relative density of the examined samples was calculated by dividing the apparent density ($\rho$) experimentally determined via the hydrostatic weighing of the samples in distilled water by their theoretical density ($\rho_{teor}$). The theoretical densities for the sintered samples with alumina additions of 0.5 or 1.0 mol% were calculated using the rule of mixtures. For dual-phase 3YSZ-$Al_2O_3$ materials, i.e. when the used amount of $Al_2O_3$ was higher than what was required to remove all the silica according to Eq. 1, the theoretical density ($\rho$) can be calculated from the following equation:

$$\rho = f_{3\,\mathrm{YSZ}} \cdot \rho_{3\,\mathrm{YSZ}} + (1 - f_{3\,\mathrm{YSZ}}) \cdot \rho_{\mathrm{Al_2O_3}} \tag{4}$$

where $f_{3\,\mathrm{YSZ}}$ is volume fraction of 3-YSZ in the sample. For the 3-YSZ that contains $x$ mol% of the unreacted $Al_2O_3$, $f_{3\,\mathrm{YSZ}}$ can be expressed using the following dependence:

$$f_{3\,\mathrm{YSZ}} = \frac{(100 - x) \cdot M_{3\,\mathrm{YSZ}} \cdot \rho_{\mathrm{Al_2O_3}}}{(100 - x) \cdot M_{3\,\mathrm{YSZ}} \cdot \rho_{\mathrm{Al_2O_3}} + x \cdot M_{\mathrm{Al_2O_3}} \cdot \rho_{3\,\mathrm{YSZ}}} \tag{5}$$

where $M$ corresponds to molar mass and theoreti-

cal density values for 3-YSZ and $Al_2O_3$ are $\rho_{3\,YSZ}$ = 6.0502 g/cm$^3$ and $\rho_{Al_2O_3}$ = 3.987 g/cm$^3$.

The silica content in the obtained 3-YSZ powder was determined using atomic absorption spectroscopy (AAS) performed by a Pye Unicum SP90P spectrometer.

The electrical properties of the two series of samples were determined via electrochemical impedance spectroscopy (EIS). The Solartron 1260 frequency response analyser and the Solartron 1294 dielectric interface were used to measure the impedance. The measurements were carried out over the frequency range from 0.1 Hz to 1 MHz, with amplitude of 10 mV and at temperatures of 550, 600, 650, 700 and 750 °C. The equivalent circuit was analysed and the values corresponding to its individual elements were established by the ZView application which came bundled with the measurement equipment. Using this software, the Kramer-Kronig (K-K) test was run for all equivalent circuits presented in the paper. Based on the obtained electrical resistance values and the geometric dimensions of the samples, the electrical conductivity values of grains ($\sigma_b$) and grain boundaries ($\sigma_{gb}$) were determined from the following dependence:

$$\sigma_{g,gb} = \frac{L}{S \cdot R} \tag{6}$$

where $R_{g,gb}$ is electrical resistance, $S$ is surface area of the platinum electrode and $L$ is sample thickness. Prior to the measurements, the surface of the samples was ground with a SiC abrasive paper with a grit size of 1000, and degreased using propanol. Platinum electrodes were then deposited on each side of the sample by screen-printing platinum paste, and fired for 2 h at 800 °C.

## III. Results

### 3.1. Structure of 3-YSZ powder

The physicochemical analyses of the 3-YSZ powder obtained via hydrothermal crystallization are shown in Fig. 1, including X-ray diffraction pattern (Fig. 1a), particle size distribution (Fig. 1b) and morphological observation (inset in Fig. 1b).

The XRD analysis showed that the 3-YSZ powder is composed of nano-sized ($D_{101}$ = 6 nm) crystallites with dominant tetragonal structure. The diffraction pattern presented in Fig. 1a indicates that, aside from the tetragonal phase with lattice parameters $a$ = 0.36152 nm and $c$ = 0.51609 nm, a small amount (4.2%) of monoclinic phase was also found. The atomic absorption spectroscopy (AAS) revealed that the concentration of silicon did not exceed 0.03 wt.%. One possible cause of the slight drop in the silicon concentration observed for the 3-YSZ powder compared to the initial zirconium oxychloride reagent (0.04124 wt.%) is the relatively high solubility of silica in alkaline solutions under hydrothermal conditions.

SEM micrograph of the 3-YSZ powder, presented in inset of Fig. 1b, indicates the presence of numerous porous agglomerates with a size ranging from around 0.1 to around 1.2 mm. BET specific surface area of this powder is 123.2 m$^2$/g, while the BET mean equivalent particle size calculated from Eq. 3 is equal to 8 nm, which is consistent with the crystallite size determined

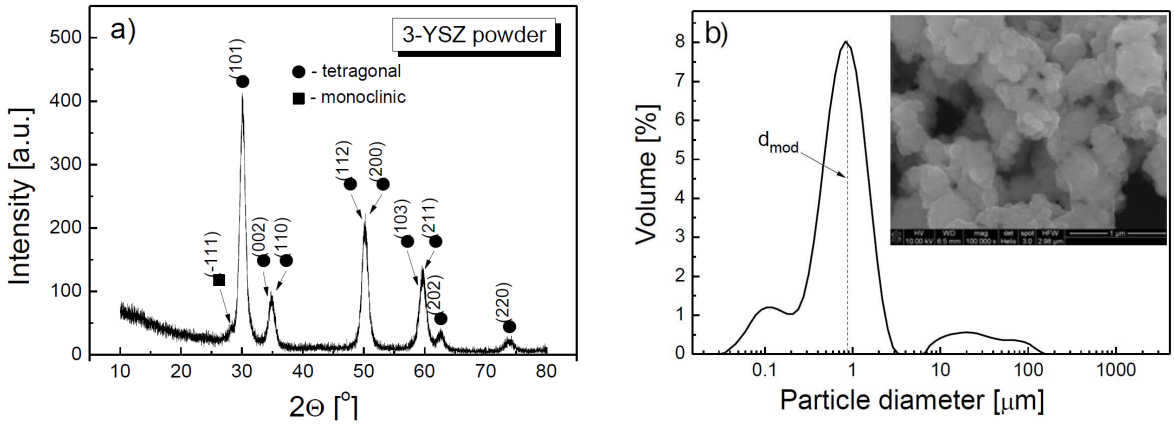


**Figure 1. Diffraction pattern (a) and particle size distribution (b) of 3-YSZ powder (SEM micrograph is shown in inset)**

**Table 1. Lattice constants $a$ and $c$ and unit cell volumes $V$ of tetragonal $ZrO_2$ phase in the studied samples depending on alumina content and sintering temperature**

| Sample | Sintering temperature: 1400 °C | | | Sintering temperature: 1500 °C | | |
|---|---|---|---|---|---|---|
| | $a$ [nm] | $c$ [nm] | $V$ [nm$^3$] | $a$ [nm] | $c$ [nm] | $V$ [nm$^3$] |
| 3Y-TZP | 0.36055(7) | 0.51768(6) | 0.06729(6) | 0.36043(6) | 0.51774(6) | 0.06725(9) |
| 3Y-TZP/0.25$Al_2O_3$ | 0.36052(3) | 0.51770(8) | 0.06728(8) | 0.36038(4) | 0.51775(5) | 0.06724(2) |
| 3Y-TZP/0.5$Al_2O_3$ | 0.36058(9) | 0.51778(1) | 0.06732(1) | 0.36036(6) | 0.51772(1) | 0.06723(1) |
| 3Y-TZP/1.0$Al_2O_3$ | 0.36048(9) | 0.51765(8) | 0.06726(6) | 0.36035(7) | 0.51772(5) | 0.06722(7) |

via XRD. The particle size distribution of the investigated 3-YSZ powder (Fig. 1b) indicates a multimodal distribution of agglomerates, of which a certain small number formed a population of so-called "hard" agglomerates. The mode value at the level of 1 μm is within the agglomerate size range estimated from the SEM micrograph (Fig. 1b).

### *3.2. Structure of 3Y-TZP and 3Y-TZP/$Al_2O_3$ samples*

*Phase composition*

Investigations of the phase composition of the samples sintered in air at 1400 or 1500 °C for 2 h, revealed the sole presence of the tetragonal form of zirconia. Table 1 shows the lattice constants and unit cell volumes of the tetragonal phase observed for the studied samples. The presented data lead to the conclusion that the observed changes in lattice constants and unit cell volumes of the tetragonal phase are small in the case of all studied samples, and they do not exceed the measurement error. This indicates that the investigated polymorphic form of zirconia exhibits an approximately constant chemical composition, regardless of the amount of added alumina and sintering temperature.

If zirconia is actually doped with alumina, a noticeable change in the lattice constants and unit cell volumes of the tetragonal phase of zirconia should have been observed due to the substitution of zirconium ions ($r_{Zr^{4+}}$ = 98 pm) with much smaller aluminium ions ($r_{Al^{3+}}$ = 67.5 pm) in the octahedral position. It therefore stands to reason that the $Al_2O_3$ addition underwent almost complete segregation at the grain boundaries of the 3Y-TZP.

*Microstructure*

In order to evaluate the influence of alumina addition on the microstructure of the sintered 3Y-TZP tetragonal zirconia obtained from the hydrothermally prepared 3-YSZ, all specimens were examined via SEM (Figs. 2 and 3). The grain size distributions are shown in the insets of these figures and the mean grain size and circularity values for two series of the investigated samples are given in Table 2.

All investigated samples were homogeneous and consisted of isometric grains, which is evident from both the grain size distribution values determined via a numerical analysis of SEM images (Figs. 2 and 3) and circularity values (Table 2). Some areas of the samples feature small pores formed due to the presence of "hard" agglomerates, which favours the growth of pores between agglomerates during the sintering of green bodies.

The grain size distributions of the samples sintered at 1400 °C are unimodal and relatively narrow (Fig. 2). They are furthermore asymmetrical, with a tendency towards grain with a larger size. It is worth noting that higher alumina content in the 3Y-TZP sample is asso-

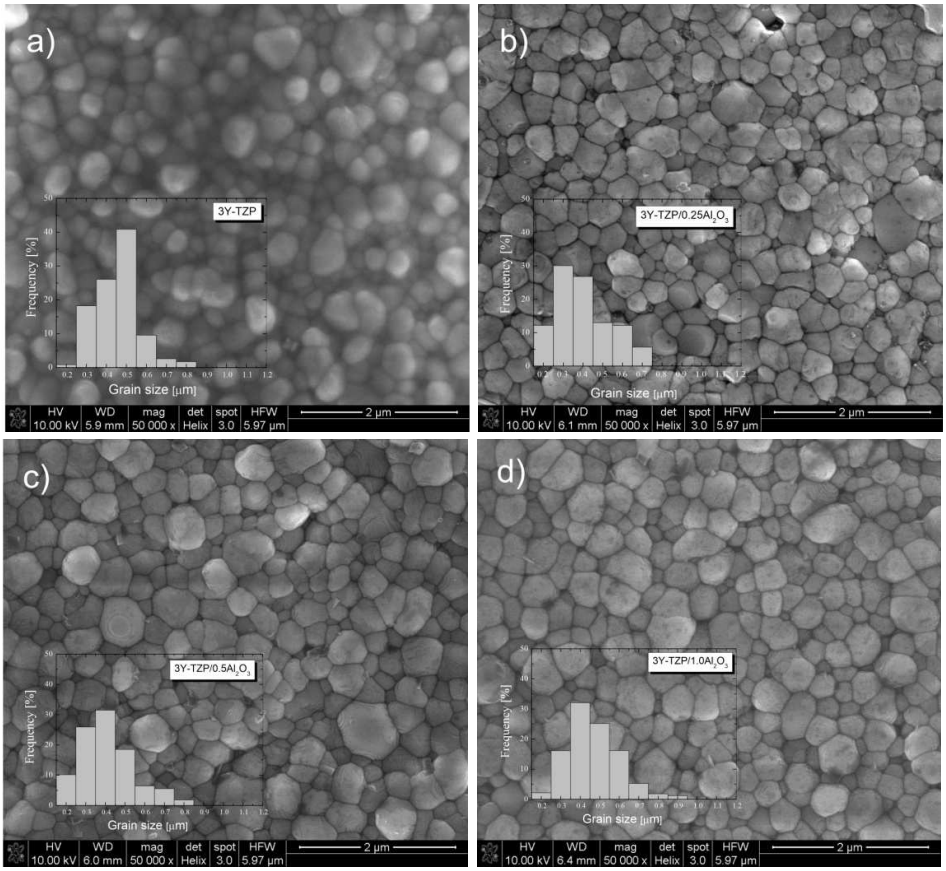


**Figure 2. SEM micrographs of specimens sintered in air at 1400 °C for 2 h: a) 3Y-TZP, b) 3Y-TZP/0.25$Al_2O_3$, c) 3Y-TZP/0.5$Al_2O_3$ and d) 3Y-TZP/1.0$Al_2O_3$ (inset: grain size distribution)**

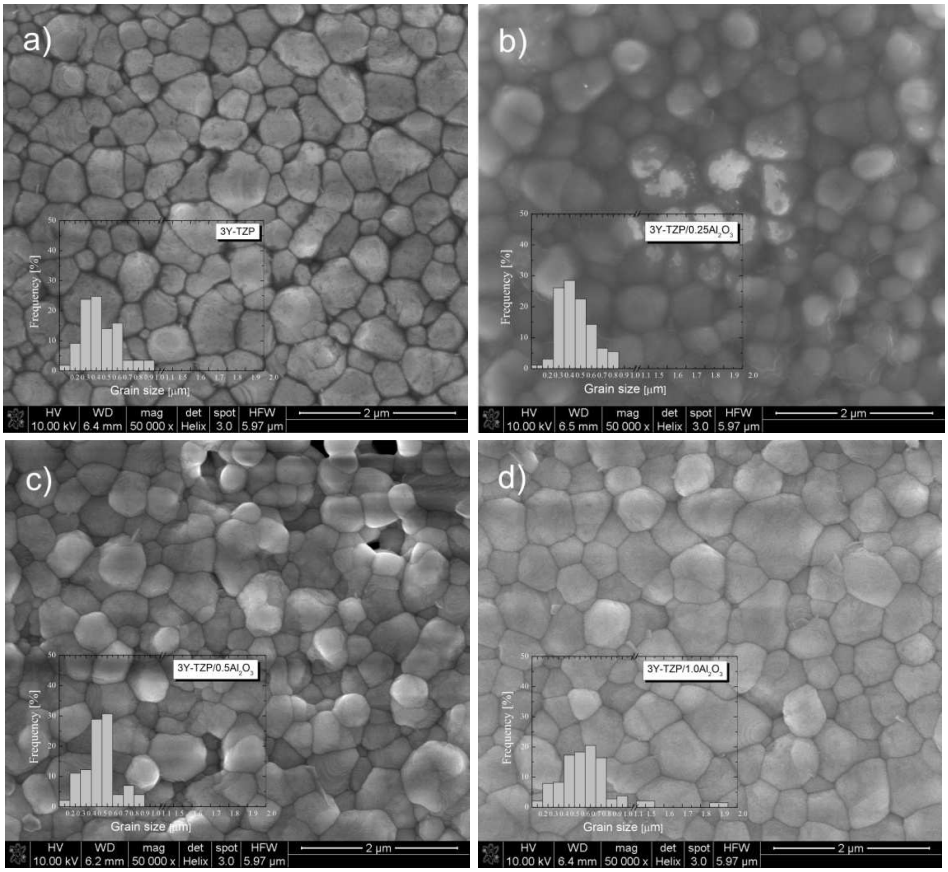


**Figure 3. SEM micrographs of specimens sintered in air at 1500 °C for 2 h: a) 3Y-TZP, b) 3Y-TZP/0.25$Al_2O_3$, c) 3Y-TZP/0.5$Al_2O_3$ and d) 3Y-TZP/1.0$Al_2O_3$ (inset: grain size distribution)**

**Table 2. Mean grain size *D* and circularity of 3Y-TZP and 3Y-TZP/$Al_2O_3$ samples depending on the alumina content and sintering temperature**

| Sample | Sintering temperature: 1400 °C | | Sintering temperature: 1500 °C | |
|---|---|---|---|---|
| | *D* [µm] | Circularity | *D* [µm] | Circularity |
| 3Y-TZP | 0.40 ± 0.11 | 0.83 ± 0.06 | 0.49 ± 0.17 | 0.85 ± 0.05 |
| 3Y-TZP/0.25$Al_2O_3$ | 0.35 ± 0.15 | 0.78 ± 0.08 | 0.49 ± 0.15 | 0.87 ± 0.06 |
| 3Y-TZP/0.5$Al_2O_3$ | 0.36 ± 0.15 | 0.79 ± 0.10 | 0.48 ± 0.16 | 0.82 ± 0.11 |
| 3Y-TZP/1.0$Al_2O_3$ | 0.41 ± 0.13 | 0.84 ± 0.07 | 0.61 ± 0.24 | 0.64 ± 0.18 |

ciated with a more narrow grain size distribution. On the other hand, thermal treatment at 1500 °C resulted in larger grains both in the case of the samples modified with alumina (3Y-TZP/$Al_2O_3$) and the unmodified 3Y-TZP sample. In addition, the size of these grains varied to a higher extent than in the case of the samples sintered at 1400 °C (Figs 2 and 3). In the case of the 3Y-TZP and 3Y-TZP/0.25$Al_2O_3$ samples sintered at 1500 °C, a unimodal, fairly wide grain size distribution was observed. For the 3Y-TZP/$Al_2O_3$ with 0.5 and 1 mol% $Al_2O_3$ the distribution is bimodal, with an asymmetry towards large-sized grains (Fig. 3).

Figure 4 shows the dependence of grain size distribution on the alumina content in the 3Y-TZP samples for both sintering temperatures. It is evident that the differences in mean grain size values observed for the samples sintered at 1400 °C are not pronounced. The smallest mean grain size of 0.35 mm was observed for the 3Y-TZP/0.25$Al_2O_3$ sample, whereas the largest one was

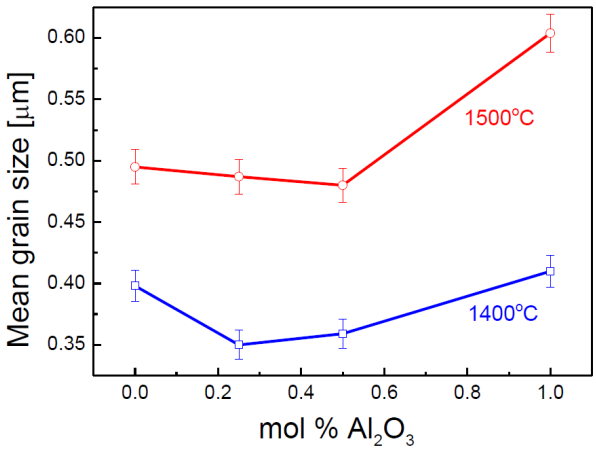


**Figure 4. Mean grain size as a function of the alumina content for 3Y-TZP samples sintered at 1400 and 1500 °C for 2 h**

**Table 3. Apparent density $\rho$ of 3Y-TZP and 3Y-TZP/$Al_2O_3$ samples and the corresponding relative density $\rho_r$**

| Sample | Sintering temperature: 1400 °C | | Sintering temperature: 1500 °C | |
|---|---|---|---|---|
| | $\rho$ [g/cm$^3$] | $\rho_r$ [%] | $\rho$ [g/cm$^3$] | $\rho_r$ [%] |
| 3Y-TZP | 5.86 ± 0.28 | 96.83 | 5.96 ± 0.46 | 98.52 |
| 3Y-TZP/0.25$Al_2O_3$ | 5.88 ± 0.62 | 97.15 | 5.99 ± 0.15 | 99.12 |
| 3Y-TZP/0.5$Al_2O_3$ | 5.79 ± 0.59 | 95.73 | 5.91 ± 0.28 | 97.86 |

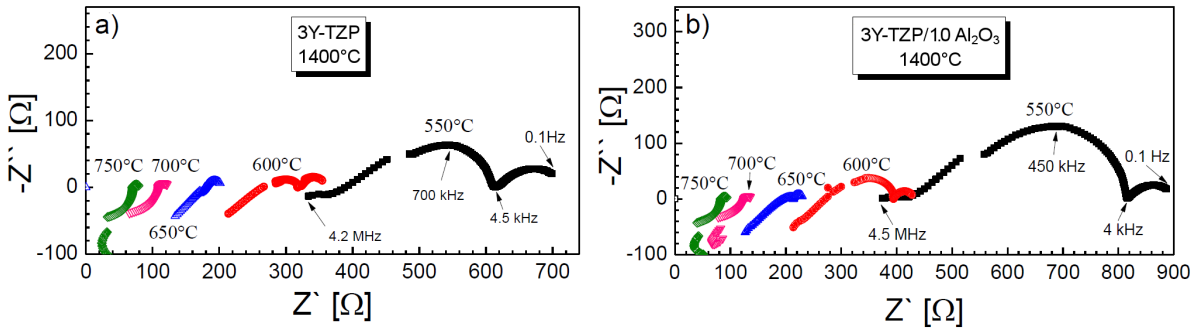


**Figure 5. Impedance spectra recorded at different temperatures for the samples sintered at 1400 °C: a) 3Y-TZP and b) 3Y-TZP/1.0$Al_2O_3$**

found in the case of the sample with 1.0 mol% of $Al_2O_3$, which was furthermore characterized by the highest circularity (Table 2). Mean grain size values for the second series of samples, sintered at 1500 °C, were higher. For these samples, a noticeable increase in the mean grain size (up to 0.61 μm) was observed for the samples with the highest alumina content (3Y-TZP/1.0$Al_2O_3$). As opposed to its counterpart sintered at 1400 °C, this particular sample exhibited the highest circularity (Table 2).

$Al_2O_3$ addition generally results in the presence of alumina inclusions, which suppress the mobility of grain boundaries and the growth of the grains of the 3Y-TZP matrix [23]. This is because grain growth is an essential condition for the change in pore geometry caused by the disintegration of neighbouring grains (the model proposed by Kellet and Lange [24,25]). In such cases, the curvature of a pore becomes convex, and the pore may undergo spontaneous elimination. In the case of the investigated samples which contained 1 mol% of alumina, the grain size increase observed in Fig. 4 may be associated with the presence of a certain concentration of inclusions in the interior of zirconia grains. This can happened because anchored inclusions "leap" over the migrating grain boundary [26]. Pawłowski and Bućko [27] demonstrated that the driving force of grain boundary migration strongly depends on the degree of curvature of grain boundaries, which in turn is highly dependent on the circularity. Consequently, the grain boundary structure in zirconia-based materials should be considered dynamic.

3Y-TZP is a candidate for application as an electrolyte in oxygen sensors and fuel cells because of its excellent thermo-mechanical properties [28] and its ionic conductivity, which is comparable or better than that of 8-YSZ [29]. It is well-known that coarse-crystalline, tetragonal $Y_2O_3$-$ZrO_2$ solid solutions are susceptible to tetragonal-to-monoclinic phase transition in the range of low temperatures (200–300 °C), which is associated with considerable changes in molar volumes [30]. This is a major disadvantage, as it leads to the deterioration of both the mechanical properties of the material and its electrical conductivity [31]. This is observed when the size of 3Y-TZP grains exceeds a certain critical value, namely ca. 0.3 μm [32]. To counteract this adverse phenomenon, Tosoh manufactures powders with a small addition of $Al_2O_3$ (TZ-3YS-E) [33].

In the case of the investigated samples, the shape of grains was mostly circular. Thus, seven out of eight analysed samples had a circularity ranging from 0.78 to 1 and the only exception was the sample with alumina addition of 1.0 mol% sintered at 1500 °C (Table 2).

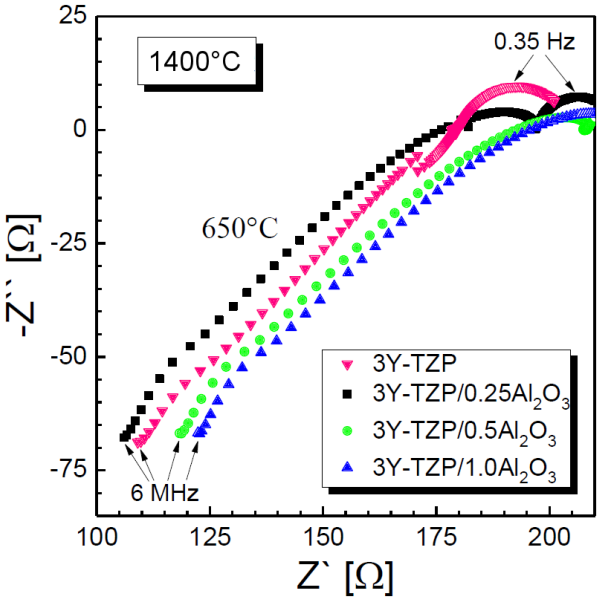


**Figure 6. Impedance spectra recorded at 650 °C for the samples sintered at 1400 °C**

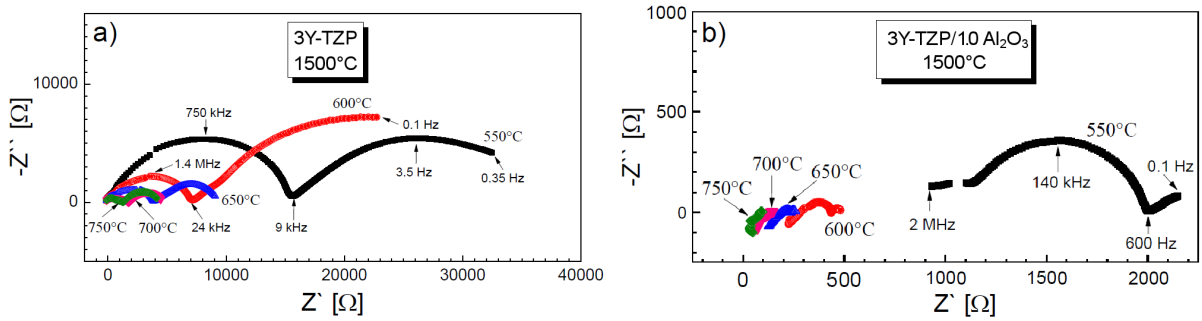


**Figure 7. Impedance spectra recorded at different temperatures for the samples sintered at 1500 °C: a) 3Y-TZP and b) 3Y-TZP/1.0$Al_2O_3$**

Based on the determined data, the 3Y-TZP/0.25$Al_2O_3$ sample sintered at 1400 °C should be considered as the most stable one.

The density of the samples (Table 3) was determined based on their relative density and total porosity. All examined samples were characterized by the relative density of over 95%. Thus the entire remaining porosity in the samples takes the form of closed porosity, and all samples should be gas-tight and thereby suitable for application as electrolyte materials for IT-SOFCs.

*Electrical conductivity*

To obtain information on the electrical properties of the prepared samples, namely the total electrical conductivity and its constituents (the electrical conductivity of grains and grain boundaries), electrical resistance was measured by means of EIS. Figure 5 shows a number of impedance spectra for pellets with the two most starkly different chemical compositions, after sintering at 1400 °C: 3Y-TZP (Fig. 5a) and 3Y-TZP/1.0$Al_2O_3$ (Fig. 5b). These measurements were performed for five temperatures ranging from 550 to 750 °C. Figure 6, on the other hand, shows the Cole-Cole plots recorded at 650 °C for the samples with different alumina content. The temperature of 650 °C was selected for two reasons: i) it is the temperature at which the impedance of the samples undergoes changes, and moreover, ii) it is the target operating temperature of a low-temperature solid oxide fuel cell (LT-SOFC). Figure 7 shows examples of the Cole-Cole plots of EIS data obtained for the 3Y-TZP and 3Y-TZP/1.0$Al_2O_3$ samples sintered at 1500 °C, while Fig. 8 presents the corresponding plots for the samples with all investigated compositions. The measurement temperatures were identical to those used for the first series of samples.

In the case of both series, the temperature increase is accompanied by changes in impedance spectra, since the material exhibits a thermally activated conduction mechanism. In the range of low temperatures up to 650 °C, the EIS spectrum is composed of two semicircles, whereas above this temperature only a single semicircle is observed. According to the accepted interpretation for zirconia-based ceramics, the first of these semicircles, which is recorded at the lowest frequencies, is associated with the transport properties of grain boundaries ($\sigma_{gb}$), whereas the second semicircle registered at the highest frequencies originates from the properties of grains ($\sigma_b$) [34,35].

In the paper by Zhang *et al.* [36], the transport properties of grain boundaries were attributed to high frequencies (ca. 1 MHz) and represented by an *RC* component in the equivalent circuit. According to that study, the grain and grain boundary conductivities can be distinguished in the Cole-Cole diagrams for 3Y-TZP. The transport properties related to grain boundaries diminish when the temperature increases. In the present paper the impedance of the experimental setup, including the device and the leads, was attributed to the lowest frequencies, as in the cited study [36]. The equivalent circuit shown in Fig. 9a was applied for all samples sintered at 1400 and 1500 °C, with the exception of the 3Y-TZP sample sintered at 1400 °C, for which the other equivalent circuit (Fig. 9b) was used.

For all samples, the imaginary part of impedance ($Z''$) assumes positive values in the range of high frequencies. This suggests a contribution of an inductive element. The presence of the inductive element can be attributed to the application of Pt electrodes. It is observed for frequencies above $10^6$ Hz [36]. The constant phase element (*CPE*) is commonly observed instead of Debye's capacitor in the case of polycrystalline samples due to the materials' inhomogeneity, porosity, electrode roughness and ionic transport deviation from Fick's law [37].

The analysis of the impedance spectra recorded over the temperature range of 550–750 °C (Figs. 5-8) made

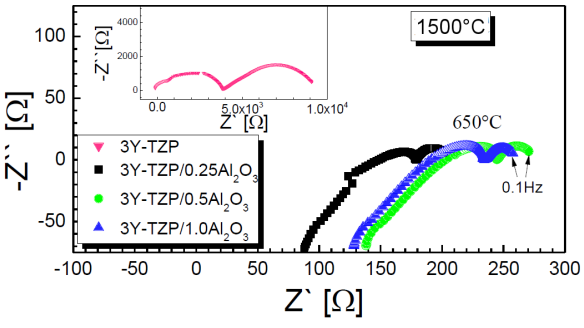


**Figure 8. Impedance spectra recorded at 650 °C for the samples sintered at 1500 °C**

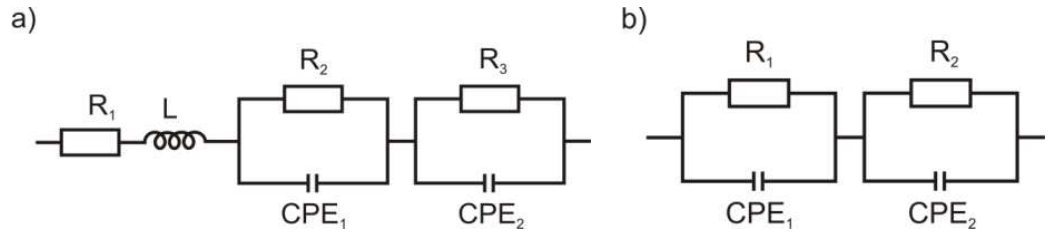


**Figure 9. Equivalent circuits for: a) samples sintered at 1400 and 1500 °C, and b) the 3Y-TZP sample sintered at 1400 °C**

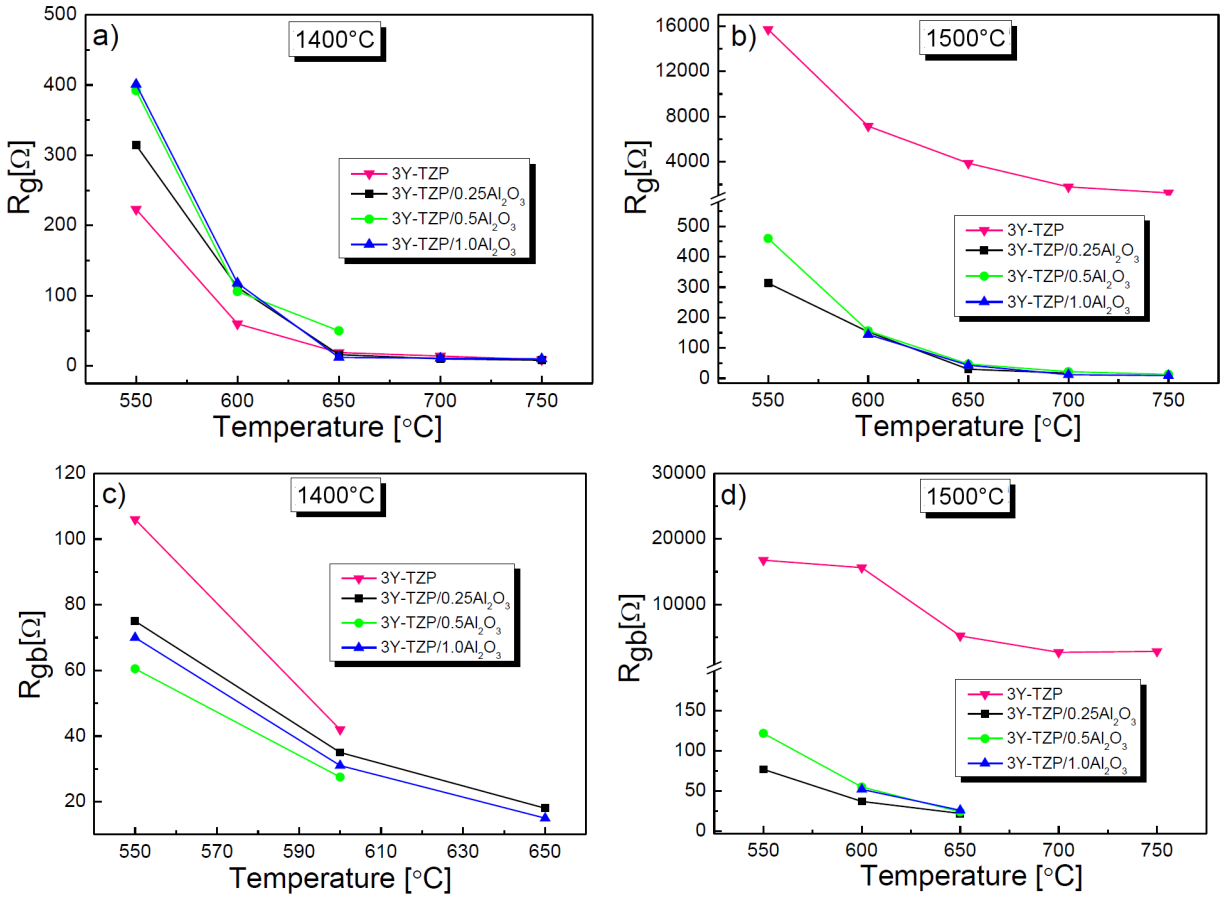


**Figure 10. Electrical resistance of grains ($R_g$) and grain boundaries ($R_{gb}$) vs. measurement temperature for the samples sintered at 1400 °C (a,c) and 1500 °C (b,d)**

it possible to determine the temperature dependence of electrical resistance of grains ($R_g$) and grain boundaries ($R_{gb}$) for all eight types of samples (Fig. 10). The data presented in Figs. 10a and 10b indicate that the effect of an alumina addition on the electrical resistance of the interior of zirconia grains depends on the microstructure of the sintered samples. In the case of the samples sintered at 1400 °C, electrical properties were worse when the measurement temperature was 550 °C; for the remaining temperatures (600–750 °C), the influence of the alumina addition on the electrical resistance of the 3Y-TZP grains was practically negligible because of the slight changes in the size of grains, which was in the range of 0.35–0.41 μm (Fig. 10a). On the other hand, in the case of the second series of samples sintered at 1500 °C (Fig. 10b), the alumina addition affected the resistance of grains to a considerable degree, since the changes in grain size (0.48–0.61 μm) were more pronounced. The electrical resistance measured for the samples modified with alumina was about two orders of magnitude lower than for the unmodified 3Y-TZP and all modified samples exhibited comparable electrical resistance regardless of sintering temperature.

In the case of the electrical resistance of grain boundaries, the tendencies were similar to those observed for the grains. For the samples sintered at 1400 °C, significant differences in electrical resistance were observed only for the lowest measurement temperature, i.e. 550 °C, while above 600 °C these differences were less pronounced (Fig. 10c). Yet again, the addition of alumina led to the significant improvements in electrical resistance in the case of the samples sintered at 1500 °C (Fig. 10d), with the exact amount added not significantly affecting the outcome.

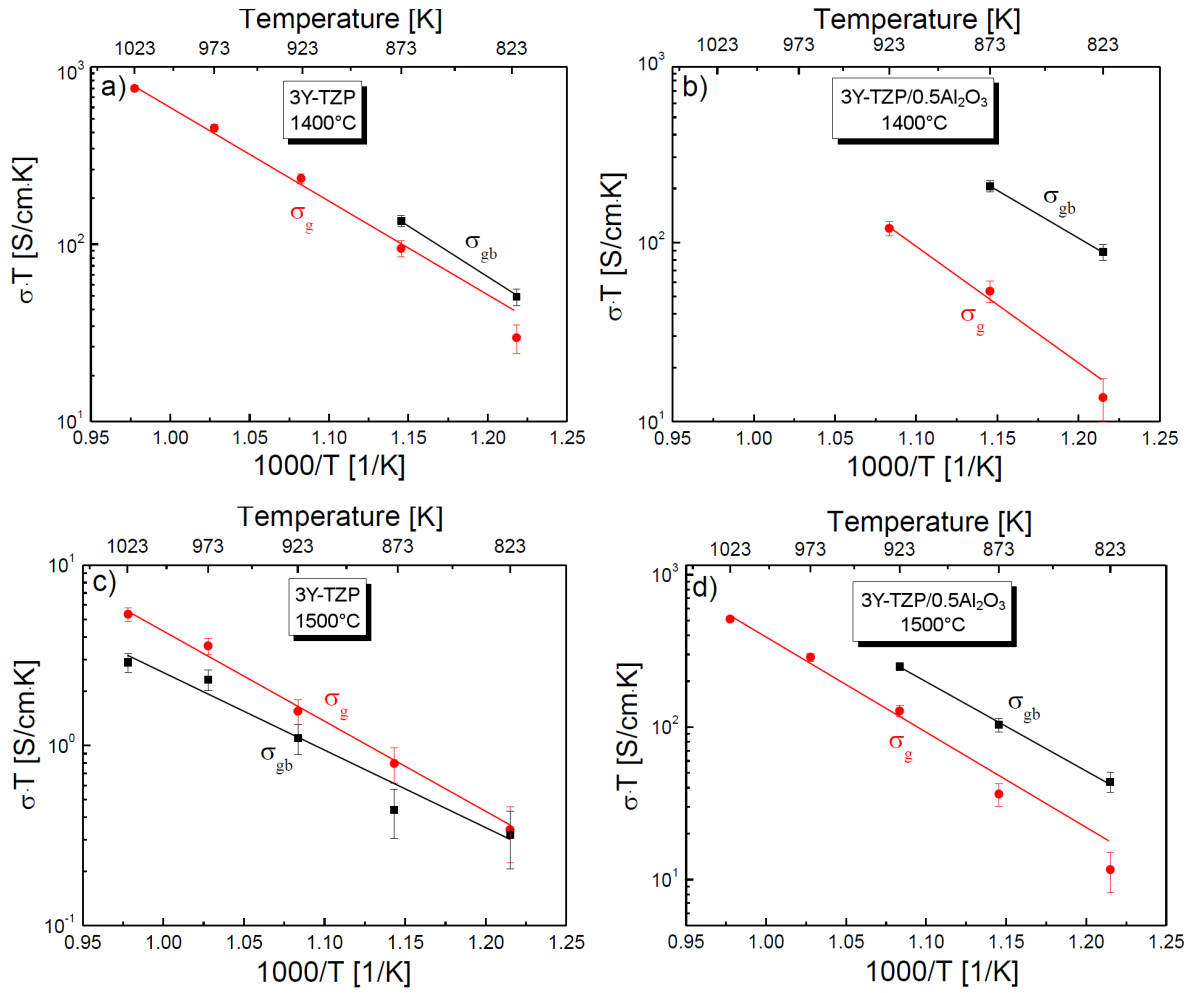


**Figure 11. Arrhenius plots showing the dependence of grain and grain boundary electrical conductivity on temperature for the sample 3Y-TZP and 3Y-TZP/0.5$Al_2O_3$ sintered at 1400 °C (a,b) and 1500 °C (c,d)**

Figure 11 shows examples of the temperature dependence of the electrical conductivity of grains ($\sigma_g$) and grain boundaries ($\sigma_{gb}$) in the form of the Arrhenius plots for the 3Y-TZP samples without any alumina addition and those with a 0.5 mol% addition, obtained after sintering at 1400 °C (Figs. 11a and 11b) and 1500 °C (Figs. 11c and 11d). The linear course of the plots leads to the conclusion that in the case of both the grains and grain boundaries electrical conduction was thermally activated. For all samples with the exception of the 3Y-TZP and 3Y-TZP/1.0$Al_2O_3$ obtained after sintering at 1500 °C, the electrical conductivity of grains ($\sigma_g$) was lower than that of grain boundaries ($\sigma_{gb}$) over the entire range of measurement temperatures (550–750 °C). The degree to which the electrical conductivity of the two constituents changed depended on the amount of added alumina and the sintering temperature. For the 3Y-TZP sample sintered at 1500 °C, these changes were slight (Fig. 11c), while the most noticeable difference was observed in the case of the 3Y-TZP/0.5$Al_2O_3$ sample sintered at 1400 °C (Fig. 11b). It is worth noting that the differences between the constituents of conduction tended to become smaller with measurement temperature. The only exception was the 3Y-TZP sample sintered at 1500 °C, for which the electrical conductivity of grains was higher than the grain boundary one at the highest temperature (Fig. 11c).

The linear character of the $ln(\sigma \cdot T) = f(1/T)$ dependence made it possible to calculate the values of the activation energy of total electrical conduction and that of both constituents, according to the following formula:

$$\sigma = \frac{\sigma_0}{T} \exp\left(-\frac{E_a}{k \cdot T}\right) \tag{7}$$

where $\sigma$ is electrical conductivity of sample, $\sigma_0$ is pre-exponential factor, $E_a$ is activation energy, $k$ is Boltzmann constant and $T$ absolute temperature. The results are presented in Table 4. The error of these calculations did not exceed 0.01 eV. The material which exhibited the lowest activation energy of grain boundary conduction was the 3Y-TZP sample without any alumina addition, regardless of the sintering temperature, whereas the highest values of this parameter were observed for the 3Y-TZP/0.5$Al_2O_3$. As far as grain conduction is concerned, the 3Y-TZP sample without any alumina addition exhibited the lowest activation energy, while the highest value was observed for the sample 3Y-TZP/1.0$Al_2O_3$.

**Table 4. Activation energies of: total $E_a(t)$, grain $E_a(g)$ and grain boundary conductivity $E_a(gb)$ for 3Y-TZP and 3Y-TZP/$Al_2O_3$ samples**

| Sample | Sintering temperature: 1400 °C | | | Sintering temperature: 1500 °C | | |
|---|---|---|---|---|---|---|
| | $E_a(t)$ [eV] | $E_a(g)$ [eV] | $E_a(gb)$ [eV] | $E_a(t)$ [eV] | $E_a(g)$ [eV] | $E_a(gb)$ [eV] |
| 3Y-TZP | 0.87 | 1.24 | 1.08 | 0.91 | 1.03 | 0.84 |
| 3Y-TZP/0.25$Al_2O_3$ | 1.04 | 1.51 | 1.01 | 0.92 | 1.51 | 0.90 |
| 3Y-TZP/0.5$Al_2O_3$ | 1.09 | 1.43 | 1.08 | 0.92 | 1.41 | 1.14 |
| 3Y-TZP/1.0$Al_2O_3$ | 0.90 | 1.52 | 1.08 | 1.15 | 1.79 | 1.04 |

**Table 5. Total $\sigma$, grain $\sigma_g$ and grain boundary conductivity $\sigma_{gb}$ measured at 650 °C for 3Y-TZP and 3Y-TZP/0.5$Al_2O_3$ sintered at 1500 °C and the commercially available 8-YSZ material produced by Tosoh as a reference [10]**

| Sample | $\sigma$ [S/cm] | $\sigma_g$ [S/cm] | $\sigma_{gb}$ [S/cm] |
|---|---|---|---|
| 3Y-TZP | $1.7 \times 10^{-3}$ | $1.2 \times 10^{-3}$ | $7.1 \times 10^{-4}$ |
| 3Y-TZP/0.5$Al_2O_3$ | $1.3 \times 10^{-1}$ | $2.7 \times 10^{-1}$ | $2.4 \times 10^{-2}$ |
| 8-YSZ (Tosoh) | $1.3 \times 10^{-5}$ | $3.2 \times 10^{-8}$ | $1.3 \times 10^{-5}$ |

Table 5 presents the values of electrical conductivity determined for the grains and grain boundaries as well as total electrical conductivity measured at 650 °C for the 3Y-TZP and 3Y-TZP/0.5$Al_2O_3$ samples sintered at 1500 °C. For comparison, data for a commercially available cubic zirconia electrolyte material (8-YSZ) supplied by Tosoh, which had been obtained after thermal treatment at 1500 °C were also added [10]. The comparison shows that the 3Y-TZP-based materials exhibit properties that are superior to those of the commercially available 8-YSZ material in terms of both constituent and total electrical conductivity. Synthesis via hydrothermal crystallization combined with the addition of alumina yields desirable properties.

*Blocking factor*

An attempt was made to determine the optimal amount of added alumina, which would allow it to effectively scavenge silica from grain boundaries and at the same time improve transport properties in these areas. The criterion selected for this purpose was the blocking factor ($f_R$), which represents the contribution of grain boundary resistivity to the total resistivity of a polycrystal, as expressed by the following equation [38]:

$$f_R = \frac{R_{gb}}{R_g + R_{gb}} \tag{8}$$

where $R_g$ and $R_{gb}$ are bulk and grain boundary resistivities, respectively. Figure 12 shows the dependence of the blocking factor on the alumina content for the samples sintered at 1400 °C (Fig. 12a) and 1500 °C (Fig. 12b).

In the case of the samples sintered at 1400 °C, the addition of alumina to the 3Y-TZP material significantly affected the blocking factor for a number of measurement temperatures. At 550 and 600 °C the blocking factor systematically decreased with $Al_2O_3$ content up to 0.5 mol%. Further increases of alumina content to 1 mol% did not cause pronounced changes in the $f_R$ value. This leads to the conclusion that the addition of 0.5 mol% is optimal with regard to the transport properties of grain boundaries. At temperatures above 600 °C, $f_R$ values are higher, which may indicate the increased contribution of grain boundary electrical conductivity to the total electrical conductivity of the samples from this series. It should be mentioned that above 650 °C it became impossible to determine the influence of the alumina addition due to the fact that only a single semicircle was formed by the impedance spectra (Figs 5 and 6).

In the case of the samples sintered at 1500 °C, increased values of $f_R$ with the increase in temperature were observed, which suggests a drop in the contribution of grain boundary electrical conductivity to the transport of electric charge. In this case, the optimal

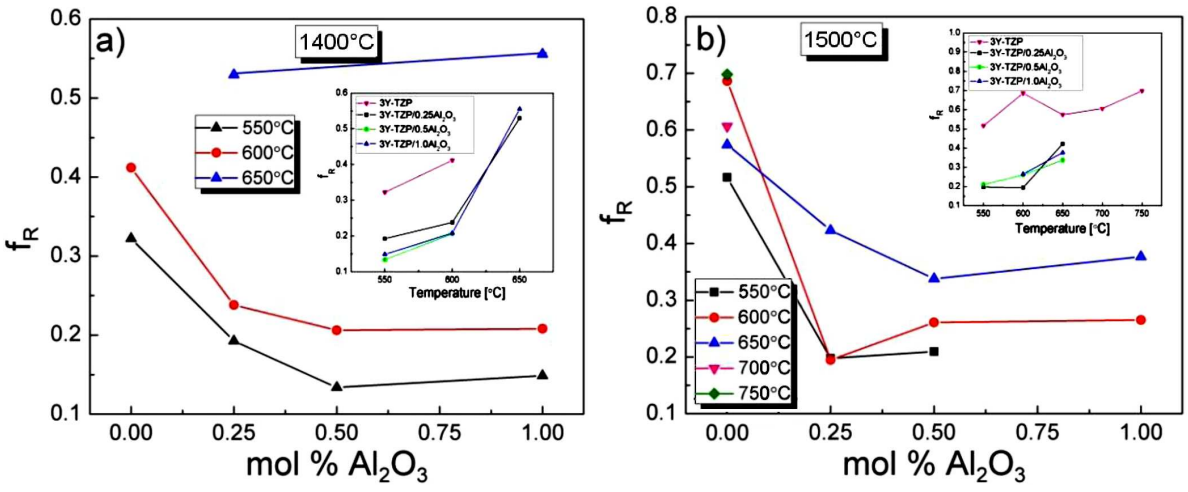


**Figure 12. Blocking factor ($f_R$) vs. $Al_2O_3$ content for the samples sintered at: a) 1400 °C and b) 1500 °C (inset: dependence of the blocking factor on the EIS measurement temperature)**

amount of alumina added to the 3Y-TZP material shifted towards lower values for a number of measurement temperatures. The unmodified sample exhibited the highest blocking factor at all measurement temperatures and, furthermore, the $f_R$ value for this sample increased slightly with temperature. In the case of the modified samples, the observed $f_R$ values did not vary significantly with alumina content at 550 and 600 °C. However, above 600 °C this factor increased independently of the amount of added alumina. It is worth stressing that the observed changes in $f_R$ values are similar for the samples from two series, and they are consistent with the conclusions of the microstructural examination of the 3Y-TZP/$Al_2O_3$ composites (Figs. 2, 3 and 4, Tables 2 and 3).

When both series of the samples are taken into account, the most desirable grain boundary transport properties at 550 and 600 °C were observed for the 3Y-TZP/0.5$Al_2O_3$ sintered at 1400 °C and the 3Y-TZP modified with 0.25 or 0.5 mol% $Al_2O_3$ sintered at 1500 °C. Consequently, these samples may be considered suitable for the role of electrolyte materials in new-generation of IT-SOFCs.

## IV. Conclusions

1. Tetragonal zirconia (3-YSZ) powder with nano-sized crystallites, obtained via hydrothermal crystallization, is a suitable for the preparation of dense 3Y-TZP/$Al_2O_3$ composites containing 0.25, 0.5 and 1.0 mol% of $Al_2O_3$ by impregnation technique and sintering at 1400 and 1500 °C.

2. There is no significant effect of alumina addition on the crystal structure and microstructure of 3Y-TZP/$Al_2O_3$ samples sintered at either 1400 or 1500 °C. However, higher densities were observed when the thermal treatment was performed at 1500 °C.

3. Alumina addition was found to affect the electrical conductivity of grains and grain boundaries in the investigated samples sintered at 1400 °C. Noticeable differences in the electrical conductivity of the two constituents can be observed for measurement temperatures of 550 and 600 °C. At these temperatures the lowest values of the blocking factor were observed for the 3Y-TZP/0.5$Al_2O_3$ composite.

4. When the thermal treatment had been performed at 1500 °C, the composite samples generally exhibited higher electrical conductivity of grain boundaries than the 3Y-TZP sample. The best grain boundary transport properties at 550 and 600 °C were determined for the 3Y-TZP samples modified with 0.25 and 0.5 mol% of $Al_2O_3$.

5. The samples which exhibited the lowest blocking factor can be considered as suitable electrolyte materials for application in IT-SOFCs.

**Acknowledgements:** The financial support of National Science Centre, grant 2016/23/B/ST8/00163 is gratefully acknowledged.

## References

1. W. Vielstisch, A. Lamm, H.A. Gasteiger, *Handbook of Fuel Cells. Fundamentals, Technology and Applications*, Wiley, Chichester, 2003.
2. S.P.S. Badwal, "Yttria tetragonal zirconia polycrystalline electrolytes for solid state electrochemical cells", *Appl. Phys. A*, **50** (1990) 449–462.
3. S.P.S. Badwal, J. Drennan, "Grain boundary resistivity in Y-TZP materials as a function of thermal history", *J. Mater. Sci.*, **24** (1989) 88–96.
4. S.P.S. Badwal, M.V. Swain, "Electrical conductivity of some fully and partially stabilized single grains", *J. Mater. Sci. Lett.*, **4** (1985) 487–489.
5. N. Bonanos, R.K. Slotwinski, B.C.H. Steele, E.P. Butler, "High ionic conductivity in polycrystalline tetragonal $Y_2O_3$-$ZrO_2$", *J. Mat. Sci. Lett.*, **3** (1984) 245–248.
6. D. Meyer, U. Eisele, R. Satet, J. Rödel, "Codoping of zirconia with yttria and scandia", *Scripta Mater.*, **58** (2008) 215–218.
7. X. Guo, Z. Zhang, "Grain size dependent grain boundary defect structure: case of doped zirconia", *Acta Mater.*, **51** (2003) 2539–2547.
8. E.P. Butler, J. Drennan, "Microstructural analysis of sintered high-conductivity zirconia with $Al_2O_3$ additions", *J. Am. Ceram. Soc.*, **65** (1982) 474–478.
9. A.J. Feighery, J.T.S. Irvine, "Effect of alumina additions upon electrical properties of 8 mol.% yttria-stabilised zirconia", *Solid State Ionics*, **121** (1999) 209–216.
10. M.C. Martin, M.L. Mecartney, "Grain boundary ionic conductivity of yttrium stabilized zirconia as a function of silica content and grain size", *Solid State Ionics*, **161** (2003) 67–79.
11. E.P. Butler, R.K. Slotwinski, N. Bonanos, J. Drennan, B.C.H. Steele, "Microstructural/electrical property relationships in high-conductivity zirconias", pp. 572–584 in *Science and Technology of Zirconia II, Advances in Ceramics Vol. 12*. Ed. by N. Claussen, M. Ruhle, A.T. Heuer, Am. Ceram. Soc., Columbus, OH, 1984.
12. K. Obal, Z. Pędzich, T. Brylewski, M. Rękas, "Modyfication of yttria-doped tetragonal zirconia polycrystal ceramics", *Int. J. Electrochem. Sci.*, **7** (2012) 6831–6845.
13. X. Guo, W. Sigle, J. Fleig, J. Maier, "Role of space charge in the grain boundary blocking effect in doped zirconia", *Solid State Ionics*, **154-155** (2002) 555–561.
14. G.D. Agnew, N.T. Hart, G.J. Wright, M. Cassidy, R.D. Collins, P.D. Butler, N. Bonanos, H.S. Thomsen, J.J. Bentzen, Y.L. Liu, A. Atkinson, R. Travis, G. Bertrand, C. Di-Pastena, C. Thompson, M.A. Henson, M.J. Day, "Scale-up of a multi-functional solid oxide fuel cell to multi-tens of kilowatt level (MF-SOFC)", *ECS Proc. Vol.*, **2003-7** (2003) 78–87.
15. J.T. Brown, "Solid Oxide Fuel Cells", pp. 630–663 in *High Conductivity Solid Ionic Conductors*. Ed. by T. Takahashi, World Scientific, Singapore, 1989.
16. X. Guo, Y. Ding, "Grain boundary space charge effect in zirconia", *J. Electrochem. Soc.*, **151** (2004) J1–J7.
17. M. Forker, P. de la Presa, W. Hoffbauer, S. Schlabach, M. Bruns, D.V. Szabó, "Structure, phase transformations, and defects of $HfO_2$ and $ZrO_2$ nanoparticles studied by $^{181}$Ta and $^{111}$Cd perturbed angular correlations, $^1$H magic-angle spinning NMR, XPS, and x-ray and electron diffraction", *Phys. Rev. B*, **77** (2008) 054108.
18. L. Liu, X. Feng, Q. Zhang, J. Xue, "ESR characterization

of $ZrO_2$ nanopowders", *J. Phys. Chem.*, **99** (1995) 332–334.
19. N.H. Perry, T.O. Mason, "Grain core and grain boundary electrical/dielectric properties of yttria-doped tetragonal zirconia polycrystal (TZP) nanoceramics", *Solid State Ionics*, **181** (2010) 276–284.
20. E. Drozdz-Ciesla, J. Wyrwa, W. Pyda, M. Rekas, "A new method of preparing Ni/YSZ cermet material", *J. Mater. Sci.*, **47** (2012) 2807–2817.
21. R.E. Riman, W.L. Suchanek, M.M. Lencka, "Hydrotermal crystallization of ceramics", *Ann. Chim-Sci. Mat.*, **27** (2002) 15–36.
22. P. Scherrer, "Nachrichten von der Gesellschaft der Wissenschaften zu Göttingen", *Mathematisch-Physikalische Klasse*, **2** (1918) 98–100.
23. F.F. Lange, T. Yamagushi, B.I. Davis, P.E.D. Morgan, "Effect of $ZrO_2$ inclusions on the sinterability of $Al_2O_3$", *J. Am. Ceram. Soc.*, **71** (1988) 446–448.
24. B.J. Kellett, F.F. Lange, "Thermodynamics of densification: I. Sintering of simple particle arrays, equilibrium configurations, pore stability, and shrinkage", *J. Am. Ceram. Soc.*, **72** (1989) 725–734.
25. F.F. Lange, B.J. Kellett, "Thermodynamics of densification: II. Grain growth in porous compacts and relation to densification", *J. Am. Ceram. Soc.*, **72** (1989) 735–740.
26. A. Nakahira, K. Niihara, "Sintering behavior and consolidation process for $Al_2O_3$/SiC nanocomposites", *J. Ceram. Soc. Jpn.*, **100** (1992) 448–453.
27. A. Pawłowski, M.M. Bućko, Z. Pędzich, "Microstructure evolution and electrical properties of yttria and magnesia stabilized zirconia", *Mater. Res. Bull.*, **37** (2002) 425–438.
28. M. Rühle, N. Claussen, A.H. Heuer, "Microstructural studies of $Y_2O_3$-containing tetragonal $ZrO_2$ polycrystals (Y-TZP)", pp. 352–370 in *Science and Technology of Zirconia II, Advances in Ceramics Vol. 12*, Am. Ceram. Soc., Columbus, OH, 1984.
29. S.P.S. Badwal, "Effect of dopand concentration on the grain boundary and volume resistivity of yttria-zirconia", *J. Mater. Sci. Lett.*, **6** (1987) 1419–1421.
30. T.K. Gupta, J.H. Bechtold, R.C. Kuznicki, L.H. Cadoff, B.R. Rossing, "Stabilization of tetragonal phase in polycrystalline zirconia", *J. Mater. Sci.*, **12** (1977) 2421–2426.
31. T.K. Gupta, R.B. Grekila, E.C. Subbaro, "Electrical conductivity of tetragonal zirconia below the transformation temperature", *J. Electrochem. Soc.*, **128** (1981) 929–931.
32. R.C. Garvie, R.H.J. Hannik, R.T. Pascoe, "Micromechanical study of the morphology of martensite in constrained zirconia", *Nature*, **258** (1975) 703–704.
33. https://www.tosoh.com/our-products/advanced-materials/zirconia-powders
34. B.C.H. Steele, "Oxygen ion conductors", pp. 402–446 in *High Conductivity Solid Ionic Conductors, Recent Trends and Applications.* Ed. by T. Takahashi, World Scientific, Singapore, 1989.
35. J.E. Bauerle, "Study of solid electrolyte polarisation by a complex admittance method", *J. Phys. Chem. Solids*, **30** (1969) 2657–2670.
36. L. Zhang, F. Liu, K. Brinkman, K.L. Reifsnider, A.V. Virkar, "A study of gadolinia-doped ceria electrolyte by electrochemical impedance spectroscopy", *J. Power Sources*, **247** (2014) 947–960.
37. E. Barsoukov, J.R. Macdonald, *Impedance Spectroscopy-Theory, Experiment and Applications*, 2nd Edn. Wiley-Interscience, 2005.
38. A.E. Hughes, S.P.S. Badwal, "An XPS investigation of impurity glass in Y-TZP", *Mater. Forum*, **15** (1991) 261–267.